

STUDY ON OPTIMUM ELECTRON BEAM WELDING CONDITIONS FOR SUPERCONDUCTING ACCELERATING CAVITIES

T. Kubo*, Y. Ajima, H. Inoue, T. Saeki, K. Umemori, Y. Watanabe, S. Yamaguchi, M. Yamanaka, KEK, 1-1 Oho, Tsukuba, Ibaraki 305-0801 Japan,
T. Nagata, ULVAC, Inc., 5-9-6 Tokodai, Tsukuba, Ibaraki, 300-2635, Japan

Abstract

Optimizations of electron beam welding conditions might solve the quench problems and improve the accelerating field of the superconducting radio-frequency cavity. As a first step toward optimum conditions, basic properties of weld beads are studied by using niobium test pieces. Effects of a combination of a beam generator position and a welding direction on geometries of weld bead are shown. Good parameter-regions for electron beam welding, which yield full penetration welds without holes or weld spatters, are surveyed. Microscopic structures, such as pits or bumps due to poor welds, have greater influence on cavity performances, which are also our research objects. We introduce a model of the magnetic field enhancement at pits, where a formula for a magnetic field enhancement factor is given as a function of parameters that express a geometry of pit. Comparisons between calculations and vertical test results are also shown.

INTRODUCTION

Accelerating field of modern superconducting radio-frequency (SRF) cavities are often limited by quenches. According to optical inspections [1] of inner surfaces of SRF cavities, a locally enhanced magnetic field at a poor electron beam welding (EBW) seam is one of causes of quenches [2]. The above observations suggest that optimizing EBW conditions to yield smooth weld bead without poor weld might solve the quench problems and improve the accelerating field of the SRF cavity.

As a first step toward optimum EBW-conditions, we study basic properties of weld beads by using niobium test-pieces. First, procedures and free EBW-parameters of this experiment are summarized. Then, typical geometries of weld beads are shown, where we see a combination of generator position and welding direction serves an important function. The good parameter-regions defined by those for full penetration welds without holes or weld spatters are shown. In addition to the above, rather microscopic structures associated with poor welds, such as pits or bumps, are also our research objects. We introduce a model of the magnetic field enhancement at pits, where a formula for a magnetic field enhancement factor is given as a function of parameters that express a geometry of pit. Then we compare the calculations and vertical test results.

*kubotaka@post.kek.jp

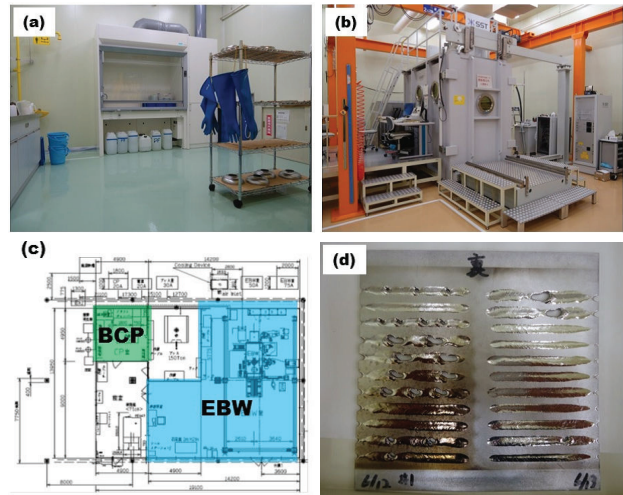


Figure 1: Cavity Fabrication Facility (CFF). (a) Chemical room. Pre-weld etchings by BCP solutions are applied in this room. (b) EBW room. Steigerwald Strahltechnik EBOCAM KS110-G150 KM-CNC is installed. (c) A sketch of the CFF. The chemical room and the EBW room are located close together. (d) An example of welded test piece. The photo shows underbeads corresponding to various combinations of EBW parameters.

EXPERIMENTS

Experiments at Cavity Fabrication Facility

Experiments are carried out at Cavity Fabrication Facility (CFF), KEK (see Fig 1(a), (b) and (c)). First, niobium test-pieces with sizes of 150 mm × 150 mm are cut out from cavity-grade niobium sheets with thickness 2.0 mm supplied from Tokyo Denkai. Then pre-weld etchings are applied to these test-pieces at the chemical room in CFF (see Fig 1(a)), where 10 – 30 μm of materials are removed by using the 1:1:1 buffered chemical polishing (BCP) solution. Following ultrapure water rinsing, etched test-pieces are carried to the next room in the CFF, where the EBW machine, Steigerwald Strahltechnik EBOCAM KS110-G150 KM-CNC, is installed (see Fig 1(b) and (c)). Then the test-pieces are welded with various combinations of EBW parameters (see Fig 1(d)), and geometries of underbeads are examined by using a surface profiler, Veeco Dektak 150.

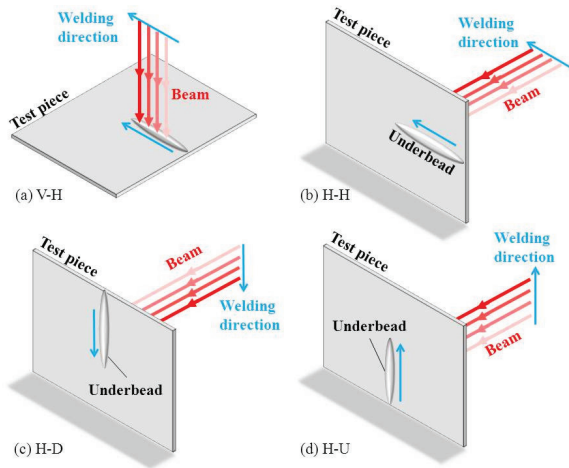


Figure 2: Schematic layouts of combinations of a generator position and a welding direction. (a) V-H: the vertical generator position and the horizontal welding direction, (b) H-H: the horizontal generator position and the horizontal welding direction. (c) H-D: the horizontal generator position and the downward welding direction, and (d) H-U: the horizontal generator position and the upward welding direction.

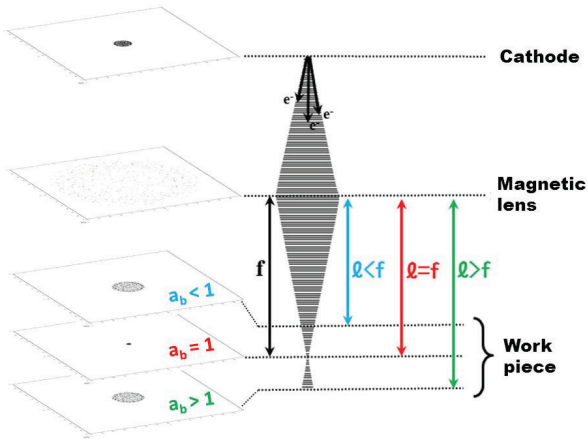


Figure 3: Examples of trajectories of electrons computed by the General Particle Tracer (GPT). Electrons emitted from the cathode go through the magnetic lens into the work piece. $\ell < f$ or $a_b < 1$ corresponds to a defocused beam: electrons are focused below the work piece. $\ell = f$ or $a_b = 1$ corresponds to a focused beam. $\ell > f$ or $a_b > 1$ also corresponds to a defocused beam: electrons are focused above the work piece.

EBW Parameters

Free EBW-parameters in this experiment are given by

- Generator position and welding direction (see Fig. 2),
- Accelerating voltage, V_a (kV),
- Beam current, I_b (mA),
- Welding speed, v (mm/s),

05 Cavity performance limiting mechanisms

H. Basic R&D bulk Nb - Other processing

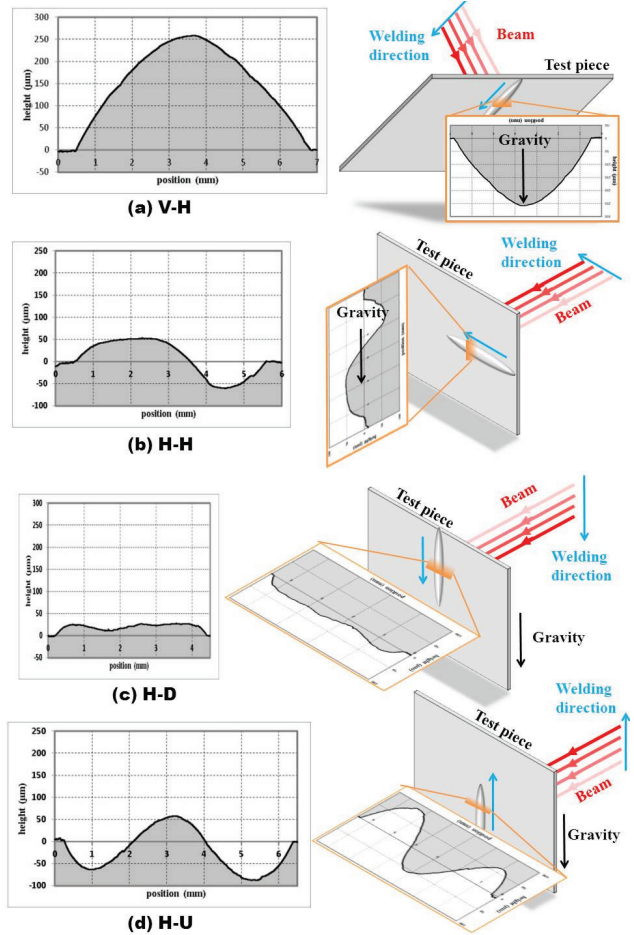


Figure 4: Typical profiles of underbead cross-sections of configurations (a) V-H, (b) H-H, (c) H-D, and (d) H-U. Schematic layouts of corresponding configurations are also shown.

- a_b -factor (see Fig. 3) .

A combination of a generator position and a welding direction, which is summarized in Fig. 3 as schematic layouts, determines a relative direction of gravity acting on molten niobium. A product $V_a I_b$ is an input beam power, and v determines an energy deposition per unit length by $V_a I_b / v$. The a_b -factor is defined by

$$a_b \equiv \frac{\ell}{f}, \quad (1)$$

where ℓ is a distance between a center of magnetic lens and a work piece. As shown in Fig. 3, the a_b -factor represents a degree of defocus, where $a_b = 1$ and $a_b \neq 1$ correspond to a focused beam and a defocused beam, respectively.

RESULTS

Geometries of Underbeads

Fig. 4(a), (b), (c), and (d) show typical profiles of underbead cross-sections for configurations V-H, H-H, H-D, and H-U, respectively. The configuration V-H yields an

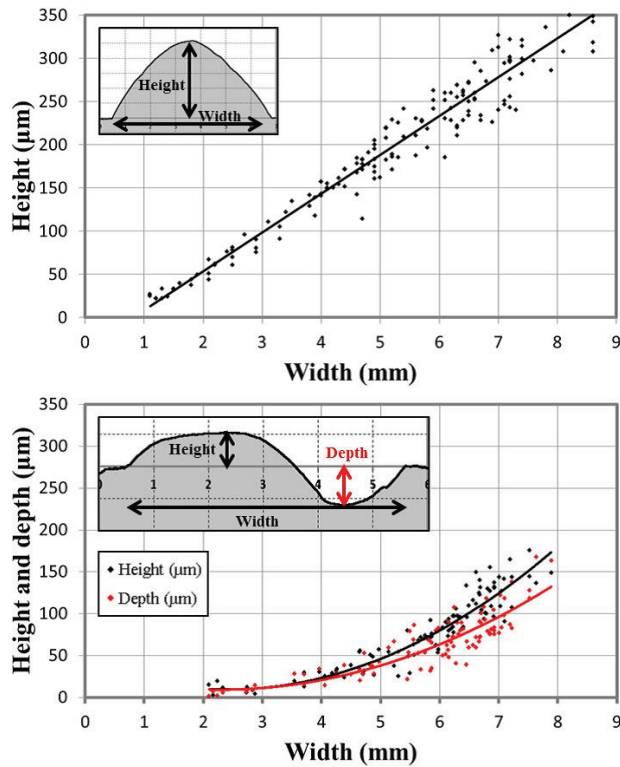


Figure 5: A relation between an underbead width and an underbead height for the configuration (a) V-H and (b) H-H with $v = 5 \text{ mm/s}$. Neither V_a , I_b , nor a_b are fixed in these plots.



Figure 6: Examples of underbeads. (a) Full penetration weld without spatters. (b) Weld bead with holes. (c) Underbead with spatters. (d) Narrow underbead.

underbead with its peak at the center. The configuration H-H yields an underbead with a swelled downside and a depressed upside. The configuration H-D yields a trapezoidal profile. The configuration H-U yields an underbead with its peak at the center and valleys on both the sides.

Fig. 5(a) shows underbead heights for configuration V-H as a function of widths, where any EBW-parameters are not fixed except for the welding speed being fixed at $v = 5 \text{ mm/s}$. An underbead height linearly increases as

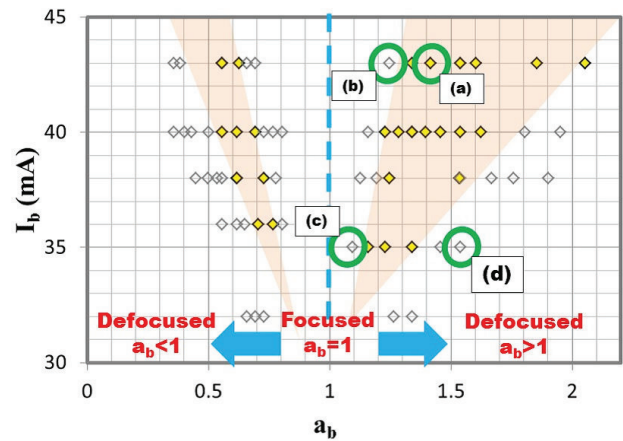


Figure 7: Good parameter-regions for configuration V-H with $V_a = 60 \text{ kV}$ and $v = 5 \text{ mm/s}$. The horizontal axis and the vertical axis represents an a_b factor and a beam current I_b (mA), respectively. The yellow symbols, which are approximately expressed by the orange-colored areas, correspond to full penetration weld without holes or weld spatters, and gray symbols correspond to poor welds such as weld beads with holes, spatters, and narrow underbeads. Characters (a), (b), (c) and (d) in the plot area correspond to Fig. 7(a), (b), (c) and (d), respectively.

a width increases. Fig. 5(b) shows underbead heights and depths for configuration H-H as a function of widths. An underbead height and depth are nearly the same magnitude, and quadratically increase as a width increases, in contrast to the linear behavior of V-H. It should be noted that the configuration V-H always yields a higher underbead than H-H with the same width.

Good Parameter Regions

As seen in Fig. 6, weld beads fall into four categories. Fig. 6(a) shows a good weld, which is a full penetration weld without holes or weld spatters. Fig. 6(b), (c) and (d) show poor welds: a weld bead with (b) holes, (c) weld spatters, and (d) a narrow underbead, where the "narrow underbead" means an underbead that is 1 mm narrower than a weld bead on the opposite side.

Fig. 7 shows good parameter-regions on a_b - I_b plane for configuration V-H with $V_a = 60 \text{ kV}$ and $v = 5 \text{ mm/s}$. The yellow symbols correspond to good weld-beads and gray symbols correspond to poor welds. Characters (a), (b), (c) and (d) in the plot area indicate EBW parameters for weld beads shown in Fig. 6(a), (b), (c) and (d), respectively. When high power beams are injected into a small area, a weld bead tends to have a larger risk of creating holes or spatters as Fig. 6(b) and (c), and Fig. 7(b) and (c). On the other hand, when beam energy is dispersed in a larger area, a weld bead tends to narrow and might be a partial penetration weld as Fig. 6(d) and Fig. 7(d). As a result, only orange-colored regions are recognized as good parameter-regions.

Fig. 8(a) shows good parameter-regions on a_b - I_b plane

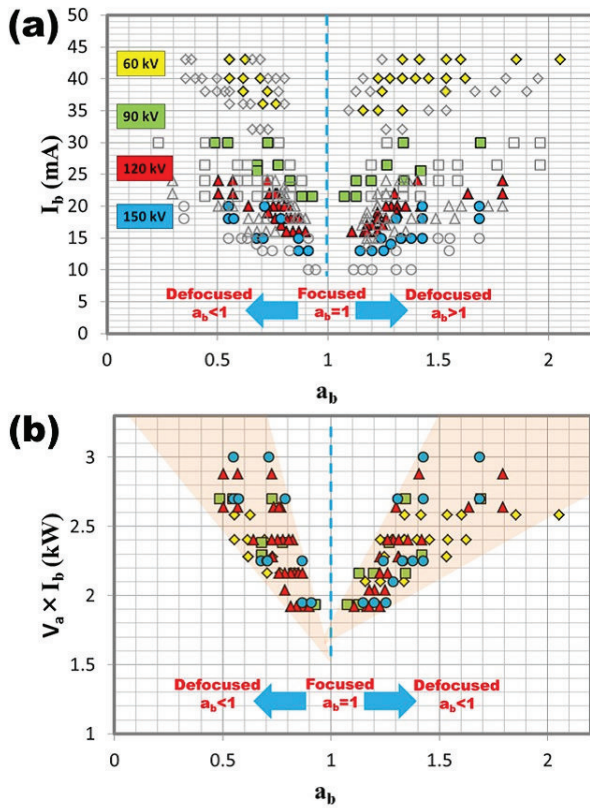


Figure 8: Good parameter-regions for configuration V-H with $v = 5$ mm/s. (a) The horizontal axis and the vertical axis represents an a_b factor and a beam current I_b (mA), respectively. (b) The horizontal axis and the vertical axis represents an a_b factor and a beam power $P = V_a I_b$ (kW), respectively. Yellow, green, red and blue symbols correspond to good parameter-regions for $V_a = 60$ kV, 90 kV, 120 kV and 150 kV, respectively.

for $V_a = 60$ kV, 90 kV, 120 kV and 150 kV, all together. As seen in the figure, I_b should be decreased as V_a increases, otherwise too much beam power make holes in a niobium test-piece. In Fig. 8(b), the same data as Fig. 8(a) are plotted on a_b - P plane, where $P = V_a \times I_b$ is a beam power. The good parameter-regions for different accelerating voltages overlap on the a_b - P plane. The orange-colored areas roughly express the good combinations of V_a , I_b , and a_b .

We only showed good parameter-regions for configuration V-H with welding speed $v = 5$ mm/s, but those for other configurations or different welding speeds are also in progress. The similar parameter search by using niobium half-cells or dumbbells are planned.

DISCUSSION ON PITS

So far we have focused on rather macroscopic structures of weld beads, such as an underbead height, depth and width, and EBW parameters for full penetration weld without spatters. However, microscopic structures, such as pits or bumps due to poor welds, have greater influence on

05 Cavity performance limiting mechanisms

H. Basic R&D bulk Nb - Other processing

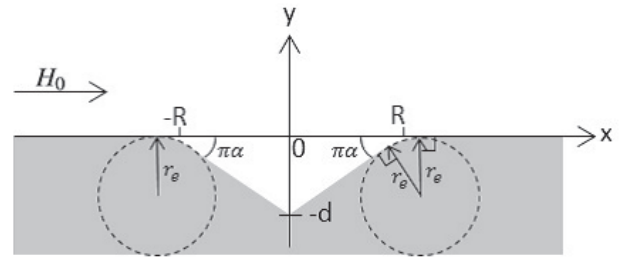


Figure 9: A two-dimensional triangular pit model with round edges. A gray region corresponds to a superconductor in the Meissner state, $\pi\alpha$ ($0 < \alpha < 1/2$) is a slope angle, R is half a width of the open mouth, and r_e is a radius of the round edge.

cavity performances, which might trigger quenches by enhancing the magnetic field. These are also our research objects. In this section, we introduce a model of the magnetic field enhancement at pits, and compare model predictions and vertical test results.

Model of the Magnetic Field Enhancement at Pit

In order to build a model of the pit, parameters that characterize a geometry of edge, such as a curvature radius and a slope angle of edge, should be included, because the magnetic field is enhanced at an edge of a pit. A shape of the bottom of the pit is not important, because the magnetic field attenuates at the bottom. The simplest model of the pit is given by the two-dimensional model with a triangular section [3, 4] shown in Fig. 9, where $\pi\alpha$, R and r_e are a slope angle, a half width and a round-edge radius, respectively. The magnetic field enhancement (MFE) factor of this model is given by

$$\beta^* = P(\alpha) \left(\frac{R}{r_e} \right)^{\frac{\alpha}{1+\alpha}}, \quad (2)$$

where $P(\alpha)$ is a coefficient depending on a slope angle α (see Ref. [4] or [5]).

Assuming that vortices start to penetrate into the defectless superconductor at $B_v \simeq 200$ mT, the achievable surface magnetic field without vortex dissipations under an existence of a pit is given by

$$B_{\text{peak}}^{(\text{pen})} = \frac{B_v}{\beta^*} = \frac{B_v}{P(\alpha)} \left(\frac{r_e}{R} \right)^{\frac{\alpha}{1+\alpha}}. \quad (3)$$

This equation is further reduced to the formula that describes the accelerating field at which vortices start to penetrate:

$$E_{\text{acc}}^{(\text{pen})} = g^{-1} B_{\text{peak}}^{(\text{pen})} = \frac{g^{-1} B_v}{P(\alpha)} \left(\frac{r_e}{R} \right)^{\frac{\alpha}{1+\alpha}}. \quad (4)$$

where g is a ratio of the peak magnetic field to the accelerating field for a given cavity-shape.

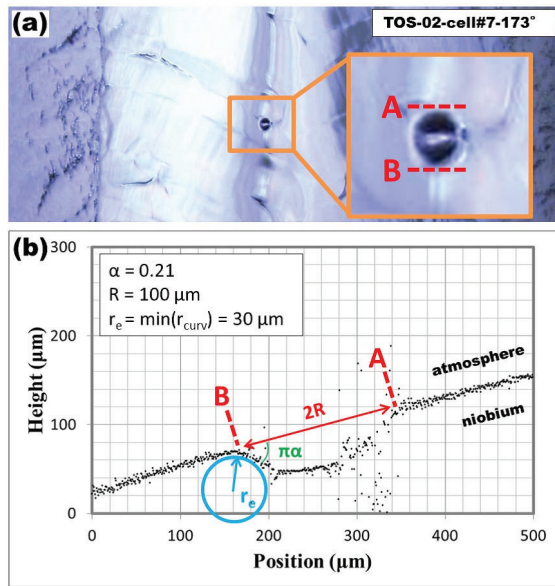


Figure 10: A pit found at the surface of TOS-02 cavity. (a) An optical image of the pit [6]. (b) Results of profilometry by a laser microscope.

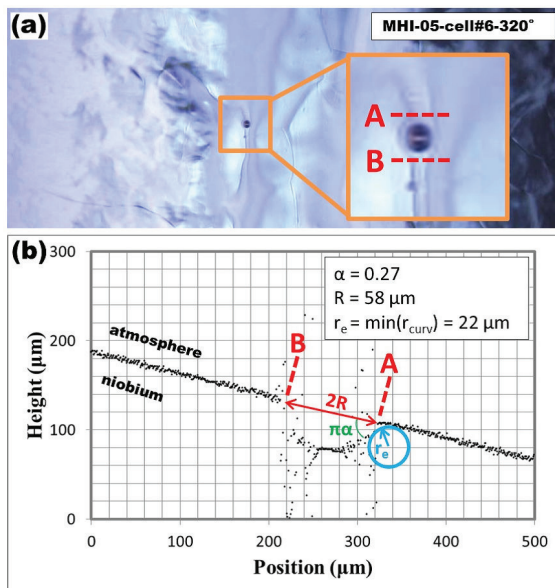


Figure 11: A pit found at the surface of MHI-05 cavity. (a) An optical image of the pit [6]. (b) Results of profilometry by a laser microscope.

Comparisons with Vertical Test Results

Fig. 10 and Fig. 11 show optical images and profiles of pits found at the surfaces of TOS-02 cavity and MHI-05 cavity. Measured values of R , r_e , and α for TOS-02 and MHI-05 are summarized in the figures, where r_e is given by the minimum value of the curvature radius r_{curv} calculated along the profile. By using these parameters, the accelerating field at which vortices start to penetrate, $E_{acc}^{(pen)}$, can be calculated from Eq. (4). Fig. 12 shows $E_{acc}^{(pen)}$ calculated from Eq. (4) and $E_{acc}^{(quench)}$, observed at vertical

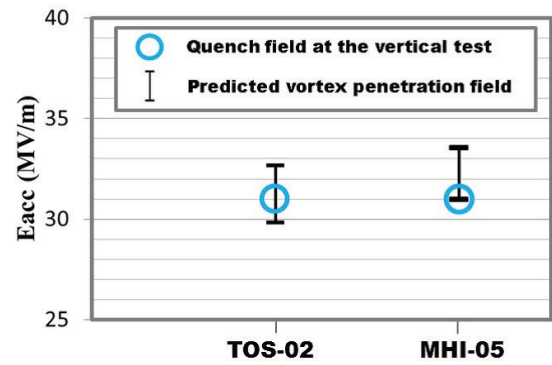


Figure 12: Comparisons between the prediction of the triangular-pit model and the vertical test results. The black bars correspond to the model-predictions, where 10% error of measured values of R , r_e , and α are assumed. The blue circles correspond to the quench fields, $E_{acc}^{(quench)}$, observed at vertical tests [2, 5-6].

tests [2, 5-6]. The agreements are remarkable, but the statistics is too small to conclude the effectiveness of the model. To accumulate statistics is a future work.

SUMMARY

As a first step toward optimum EBW-conditions, we study basic properties of weld beads. In this paper, we mentioned following three topics:

- effects of a combination of a beam generator position and a welding direction on geometries of weld bead for niobium test-pieces,
- good parameter-regions for electron beam welding that yield full penetration welds without holes or weld spatters for niobium test-pieces,
- a theoretical study on a relation between a magnetic field enhancement factor and a geometry of a pit, and comparisons between the theory and vertical test results.

Regarding the second topic, we only showed good parameter-regions for configuration V-H with welding speed $v = 5$ mm/s, but those for other configurations or different welding speeds are also in progress. Regarding the third topic, the statistics is too small to conclude the effectiveness of the model. To accumulate statistics is a future work.

ACKNOWLEDGEMENTS

The author would like to express my gratitude to Yasuchika Yamamoto for his providing the experimental data and fruitful discussions.

REFERENCES

[1] Y. Iwashita, Y. Tajima, and H. Hayano, Phys. Rev. ST Accel. Beams 11, 093501 (2008).

- [2] Yasuchika Yamamoto, Nucl. Instrum. Methods Phys. Res. A 623, 579 (2010).
- [3] Takayuki Kubo, arXiv:1307.5943 [physics.acc-ph].
- [4] Takayuki Kubo, in Proceedings of this conference.
- [5] Yasuchika Yamamoto, in Proceedings of this conference.
- [6] Yasuchika Yamamoto, private communications.